Fourier coefficients of the net baryon number density and chiral criticality

Gábor András Almási,[1] Bengt Friman,[2] Kenji Morita,[3,4] Pok Man Lo,[3] and Krzysztof Redlich[3,5]

[1]*Wigner Research Center for Physics, H-1121 Budapest, Hungary*
[2]*GSI Helmholtzzentrum für Schwerionenforschung GmbH, D-64291 Darmstadt, Germany*
[3]*Institute of Theoretical Physics, University of Wrocław, PL-50204 Wrocław, Poland*
[4]*iTHES Research Group, RIKEN, Saitama 351-0198, Japan*
[5]*Research Division and EMMI, GSI Helmholtzzentrum für Schwerionenforschung,*
64291 Darmstadt, Germany

We investigate the Fourier coefficients $b_k(T)$ of the net baryon number density in strongly interacting matter at nonzero temperature and density. The asymptotic behavior of the coefficients at large k is determined by the singularities of the partition function in the complex chemical potential plane. Within a QCD-like effective chiral model, we show that the chiral and deconfinement properties at nonzero baryon chemical potential are reflected in characteristic k- and T-dependencies of the Fourier coefficients. We also discuss the influence of the Roberge-Weiss transition on these coefficients. Our results indicate that the Fourier expansion approach can provide interesting insights into the criticality of QCD matter.

I. INTRODUCTION

Exploring the phase diagram of quantum chromodynamics (QCD) at finite temperature and chemical potentials is a challenging problem in experimental and theoretical studies. The Beam Energy Scan (BES) at the Relativistic Heavy Ion Collider (RHIC) [1] has been dedicated to the search for the conjectured QCD critical point (*CP*) and the onset of deconfinement through the systematic studies of various observables such as the fluctuations of conserved charges. In particular, those of the net-proton number have been shown to exhibit a nonmonotonic behavior with collision energies which may potentially be attributed to critical chiral dynamics [2–9].

Fluctuation observables can also be computed in lattice QCD (LQCD) [10–12] and in effective chiral models [5,9,13–15]. Thus, by identifying fluctuation patterns, associated with chiral critical behavior, in experimental data, one may be able to identify the QCD phase boundary and the location of the *CP*, if it exists [2,5,9,16,17].

While LQCD provides first principle insights into the thermodynamics of QCD at finite temperature T and at vanishing and moderate values of the baryon chemical potential $\mu_B < 3T$, the well-known sign problem still inhibits systematic calculations at larger baryon densities.

Several strategies to overcome this problem are being pursued [18,19].

In particular, LQCD calculations at imaginary baryon chemical potential offer a possibility to circumvent the sign problem at real μ_B. On the one hand, these calculations, which do not suffer from the sign problem, can, in principle, be analytically continued to the real axis [20–22]. On the other, a Fourier expansion in imaginary μ_B can be applied to the partition function in order to study the properties, in particular the phase structure, of QCD at finite baryon density in the canonical ensemble [23–26]. Moreover, the canonical partition function can be used to obtain the probability distribution function $P(N)$ of the net baryon number N, which in turn yields the cumulants of the net baryon number fluctuations [27–33]. As noted in Ref. [31], knowledge of the probability for large-amplitude fluctuations, i.e., fluctuations with large N, is required for a correct identification of the critical properties associated with the chiral phase transition.

Furthermore, a novel strategy for locating the confinement-deconfinement transition by exploring the complex phase of the Polyakov loop at imaginary chemical potential has been proposed in [34,35]. Thus, by studying QCD at imaginary chemical potential, one can gain insight into the critical properties of QCD related to deconfinement, chiral symmetry restoration and the Roberge-Weiss transition.

In this paper we explore the Fourier decomposition of the (dimensionless) net baryon number density

$$\chi_1^B(T, \hat{\mu}_B) \equiv \frac{n_B(T, \hat{\mu}_B)}{T^3} = \frac{\partial(p/T^4)}{\partial \hat{\mu}_B}, \qquad (1)$$

where $p = p(T, \hat{\mu}_B)$ is the pressure, $\hat{\mu}_B = \mu_B/T$ is the reduced baryon chemical potential and T the temperature. The analytic continuation of χ_1^B to imaginary baryon chemical potential is an odd, periodic function of $\theta_B = \text{Im}\hat{\mu}_B$, and can thus be expanded in a Fourier sine series:

$$\text{Im}[\chi_1^B(T, i\theta_B)] = \sum_{k=1}^{\infty} b_k(T) \sin(k\theta_B). \qquad (2)$$

The aim of our study is to identify the influence of chiral symmetry restoration and deconfinement on the Fourier coefficients $b_k(T)$. We examine the effects of criticality by making use of QCD-like chiral effective models. In particular, we discuss the effect of singularities in the complex chemical potential plane associated with first- and second-order phase transitions, crossover transitions and the contribution of the so-called thermal singularities. Model-independent results will be reported in a separate publication [36].

To be specific, we employ the two-flavor Polyakov-quark-meson (PQM) model, which emulates the characteristic properties of QCD both at real [37] and imaginary [38] baryon chemical potentials. At nonzero T and $\theta_q = \theta_B/N_c$, the resulting thermodynamic potential exhibits chiral symmetry restoration and statistical confinement, as well as the Roberge-Weiss symmetry [39], which implies a periodicity of $2\pi/N_c$ in θ_q.

We show that the k- and T-dependencies of the Fourier coefficients $b_k(T)$ exhibit characteristic features, reflecting the chiral and Roberge-Weiss transitions at imaginary baryon chemical potential.

The results are discussed in light of the Fourier expansion coefficients that were recently obtained in LQCD simulations at imaginary chemical potential for a wide range of temperatures around and above the chiral and deconfinement transitions [40]. Furthermore, we examine the recently proposed cluster expansion model [41] for Fourier coefficients and discuss its predictive power and analytic properties in the context of chiral criticality.

The paper is organized as follows: In the next section, we analyze phenomenological models for the Fourier coefficients and their applicability to the description of criticality and interpretation of recent LQCD results. The properties of the Fourier expansion coefficients in a QCD-like effective chiral model are examined in Sec. III. Finally, Sec. IV is devoted to a summary and conclusions.

II. MODELING THE FOURIER COEFFICIENTS AND LATTICE QCD

A. Models for Fourier coefficients

A model for the Fourier coefficients of the net baryon density, the cluster expansion model (CEM), was recently proposed in Ref. [41]. Based on the popular hadron-resonance gas equation of state with excluded-volume

corrections, the authors suggested a simple prescription for computing the higher-order Fourier coefficients of the net baryon density $b_k(T)$ in Eq. (2) in terms of the first two, $b_1(T)$ and $b_2(T)$,

$$b_k^{\text{CEM}}(T) = \left(\frac{b_1^{SB}}{b_1(T)}\right)^{k-2} \left(\frac{b_2(T)}{b_2^{SB}}\right)^{k-1} b_k^{SB}, \qquad (3)$$

where

$$b_k^{SB} = (-1)^{k-1} \frac{12 + 16(\pi k)^2}{27k(\pi k)^2} \qquad (4)$$

are the Fourier coefficients of the density of a noninteracting gas of massless quarks with $N_c = 3$ colors and $N_f = 3$ flavors. The coefficients (3) are constructed such that they all approach the corresponding Stefan-Boltzmann (SB) values (4), when $b_1(T)$ and $b_2(T)$ approach b_1^{SB} and b_2^{SB}, respectively.

The first four Fourier coefficients, $b_1(T) - b_4(T)$, have been obtained in LQCD calculations [40]. It was shown in Ref. [41] that Eq. (3), using the lattice results as input for $b_1(T)$ and $b_2(T)$, provides a description of $b_3(T)$ and $b_4(T)$ consistent with LQCD. Furthermore, the model predictions for the temperature dependence of the sixth-order baryon number susceptibility are qualitatively consistent with LQCD findings.

Thus, the CEM describes the basic features of the available lattice results on baryon number fluctuations. Nevertheless, one may ask whether the critical behavior of QCD associated with the restoration of chiral symmetry, which is reflected in the asymptotic behavior of the Fourier coefficients, can be captured by the model. More generally, it is of interest to assess to which extent the modeling of Fourier coefficients is unique, when only the first two coefficients are provided as input.

In order to illustrate these issues, we introduce an alternative model, which we dub the "rational fraction model" (RFM). The functional form of the RFM Fourier coefficients,[1]

$$b_k^{\text{RFM}}(T) = \frac{c(T)}{1 + \sqrt{k^2}/k_0(T)} b_k^{SB}, \qquad (5)$$

with

$$k_0(T) = \left[\frac{b_1(T)b_2^{SB}}{b_2(T)b_1^{SB}} - 1\right]^{-1} - 1, \qquad (6)$$

---

[1]Note that the prefactor in (5) is an even function of k and thus preserves the symmetry of the sine Fourier coefficients (4), i.e., $b_{-k}^{\text{RFM}} = -b_k^{\text{RFM}}$.
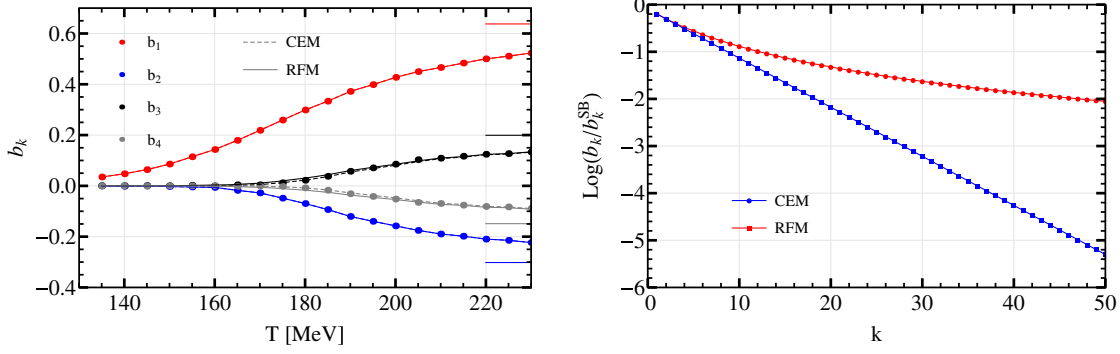
FIG. 1.   Left: Temperature dependence of the Fourier coefficients in the cluster expansion model (CEM) [41] and the rational function model (RFM), defined in Eq. (5), compared to LQCD data [40]. Right: The Fourier expansion coefficients obtained in these models at $T = 230$ MeV.

$$c(T) = \frac{b_1(T)}{b_1^{SB}} \left(1 + \frac{1}{k_0(T)} \right), \qquad (7)$$

was chosen so that the asymptotics is a power law and the SB limit as well as the lattice results on Fourier coefficients are reproduced. By contrast, the CEM Fourier coefficients (3) fall off exponentially for $k \to \infty$. In the left panel of Fig. 1, we show the temperature dependence of the CEM and RFM Fourier coefficients $b_1 \ldots b_4$. The overall agreement with the LQCD results [40] is of similar quality for the two models.

The asymptotic behavior of the Fourier coefficients in the CEM and RFM is illustrated in the right panel of Fig. 1. As discussed below, the change from exponential to power-law asymptotics of the Fourier coefficients is a consequence of a different analytical structure of the density in the complex chemical potential plane and is also reflected in modifications of higher cumulants of the net baryon number. This example illustrates the fact that the asymptotic form of a Fourier series and consequently the analytic structure of the function are not fixed by the first few Fourier coefficients.

For real values of the baryon chemical potential, the net baryon number density (1) is given by

$$\chi_1^B(T, \hat{\mu}_B) = \sum_{k=1}^{\infty} b_k(T) \sinh(k\hat{\mu}_B), \qquad (8)$$

where $\hat{\mu}_B = \mu_B/T$ and $b_k(T)$ are the Fourier coefficients of the density at imaginary chemical potential (2),

$$b_k(T) = \frac{2}{\pi} \int_0^{\pi} d\theta_B [\text{Im}\chi_1^B(T, i\theta_B)] \sin(k\theta_B). \qquad (9)$$

Higher-order fluctuations of the net baryon number are obtained by taking derivatives of Eq. (8),

$$\chi_n^B = \sum_{k=1}^{\infty} b_k \frac{\partial^{n-1}}{\partial \hat{\mu}_B^{n-1}} \sinh(k\hat{\mu}_B). \qquad (10)$$

In Fig. 2 we show $\text{Im}[\chi_1^B(T, i\theta_B)]$, obtained with Eq. (2) using the Fourier coefficients (3) and (5) at several temperatures. Since the first four coefficients coincide in CEM and RFM, the difference between the two models for the baryon number density at imaginary chemical potential is relatively small and discernible only at $\theta_B \simeq \pi$. There, by construction, both functions drop rapidly to zero and the convergence of the Fourier sum is slow.

Differences between the higher-order Fourier coefficients imply very different predictions for the baryon number susceptibilities χ_n^B, in particular at large n.

In Fig. 3 we show the fourth- and tenth-order cumulants normalized by χ_2^B in CEM and RFM. Each point represents the result of a model calculation, where the Fourier coefficients were obtained using Eqs. (3)–(7), respectively, while $b_1(T)$ and $b_2(T)$ are given by LQCD data. The lines in Fig. 3 are obtained by interpolating the LQCD values for $b_1(T)$ and $b_2(T)$ as functions of temperature in the range $T \in [165 \text{ MeV}, 220 \text{ MeV}]$. We thus obtain the following fit to the LQCD data:
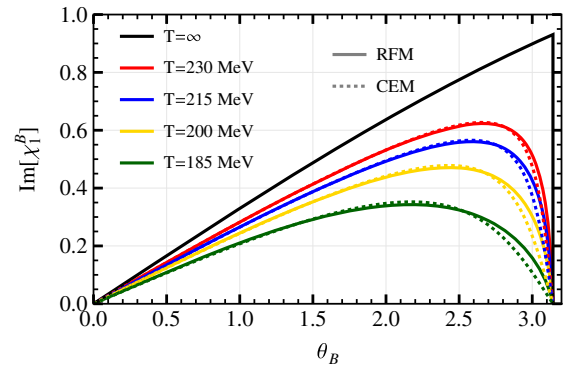

FIG. 2.   The imaginary part of the baryon density at imaginary baryon chemical potential for various temperatures obtained in the rational function model (RFM) and cluster expansion model (CEM).
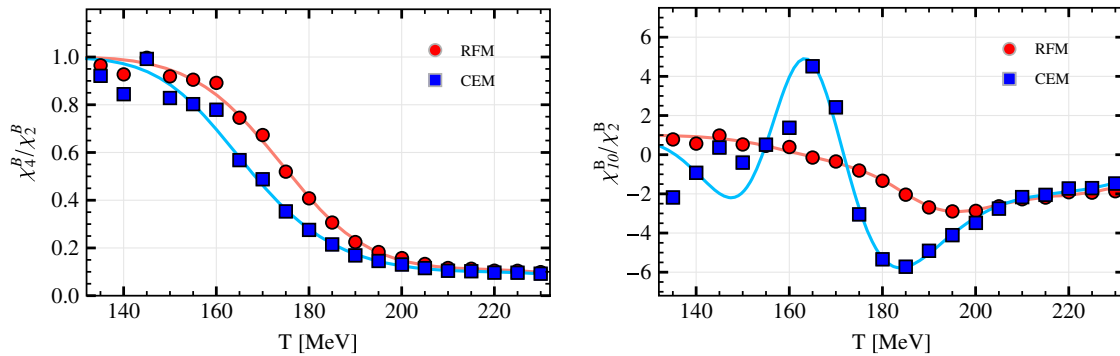
FIG. 3. Baryon number cumulant ratios obtained in the cluster expansion model [41] and the rational function model of Eq. (5). The points are computed directly using the LQCD data points [40] for b_1 and b_2 and the two models for the higher-order Fourier coefficients. The solid curves were obtained by fitting b_1 and b_2 to the LQCD data, as described in the text.

$$\log(b_1) = -41.5 + 83.1x - 56.8x^2 + 13.1x^3,$$
$$\log(-b_2) = -135.4 + 280.2x - 196.4x^2 + 46.1x^3, \quad (11)$$

with $x = T/155$ MeV.

As shown in the left panel of Fig. 3, the two models yield similar behavior for the temperature dependence of the χ_4^B/χ_2^B ratio. However, higher-order cumulants are very different in these models due to the contribution of higher-order Fourier coefficients. This is illustrated in the right panel of Fig. 3 where we show that the temperature dependence of the χ_{10}^B/χ_2^B ratio in CEM and RFM differs essentially in the crossover region. This clearly demonstrates that the characteristic features of higher-order fluctuations, which are sensitive to criticality, are not uniquely determined by requiring that the first four Fourier coefficients be reproduced. Thus, in contrast to Ref. [41], we find that models of this type are in general not suited for exploring chiral criticality.

In fact, in the following we show that for the phenomenological CEM the Fourier series in Eq. (2) can be resummed and expressed by the polylogarithm functions which have well-defined analytic structure, excluding explicitly any information on criticality expected in QCD. This is also the case for the RFM.

B. Analytic properties and criticality

Given the Fourier coefficients of the net baryon density, one can compute susceptibilities and consequently obtain information on the location of singularities in the complex μ_B plane, e.g., by computing the radius of convergence of the Taylor expansion of the pressure. In order to assess whether the CEM exhibits any singularities that could provide insight into the critical behavior of QCD, we examine the analytical properties of the model. Of particular interest in this context are the questions concerning the location of singularities associated with the QCD chiral transition.

We first consider the Fourier expansion of the density in the CEM in the Stefan-Boltzmann (SB) limit. In this case, the baryon density is computed using the Fourier coefficients (4) in (8),

$$\chi_1^{B,SB} = \sum_{k=1}^{\infty} b_k^{SB} \sinh(k\hat{\mu}_B)$$
$$= \frac{2}{27\pi^2} \sum_{s=\pm 1} s \left[3 \sum_{k=1}^{\infty} \frac{(-e^{-s\hat{\mu}_B})^k}{k^3} + 4\pi^2 \sum_{k=1}^{\infty} \frac{(-e^{-s\hat{\mu}_B})^k}{k} \right]$$
$$= \frac{2}{27\pi^2} \sum_{s=\pm 1} s[3\mathrm{Li}_3(-e^{-s\hat{\mu}_B}) - 4\pi^2 \log(1 + e^{-s\hat{\mu}_B})],$$
$$(12)$$

where $\mathrm{Li}_n(z)$ denotes the polylogarithm of order n defined by

$$\mathrm{Li}_n(z) = \sum_{k=1}^{\infty} \frac{z^k}{k^n}. \quad (13)$$

We note that Eq. (12) is valid also for complex values of the chemical potential. Moreover, for $|\mathrm{Im}\hat{\mu}_B| < \pi$, Eq. (12) reduces to

$$\chi_1^{B,SB} = \frac{\hat{\mu}_B}{3} + \frac{\hat{\mu}_B^3}{27\pi^2}, \quad (14)$$

while for $|\mathrm{Im}\hat{\mu}_B| > \pi$, the function is consistent with the periodicity in the imaginary $\hat{\mu}_B$ direction, which is implemented in the model.

Now, the density of an ideal gas of massless quarks and antiquarks is given by the well-known expression

$$\chi_1^{B,IG} = \frac{2N_c N_f}{3} \int \frac{d^3\hat{p}}{(2\pi)^3} \left(\frac{1}{1 + e^{\hat{p}-\hat{\mu}_B/3}} - \frac{1}{1 + e^{\hat{p}+\hat{\mu}_B/3}} \right)$$
$$= \frac{2N_c N_f}{3\pi^2} (\mathrm{Li}_3(-e^{-\hat{\mu}_B/3}) - \mathrm{Li}_3(-e^{\hat{\mu}_B/3})), \quad (15)$$

where $\hat{p} = p/T$. For $|\mathrm{Im}\hat{\mu}_B| < 3\pi$, Eq. (15) reduces to the polynomial form (14). Consequently, $\chi_1^{B,SB}$ and $\chi_1^{B,IG}$ coincide within a band in the complex $\hat{\mu}_B$ plane defined by $|\mathrm{Im}\hat{\mu}_B| < \pi$ (as well as in bands obtained by shifting $\mathrm{Im}\hat{\mu}_B$ by multiples of 6π).

Outside these bands, the two densities differ, due to the different periodicities: $\chi_1^{B,SB}$ is invariant under translations of the baryon chemical potential by multiples of $2\pi i T$, i.e., $\hat{\mu}_B \rightarrow \hat{\mu}_B + 2\pi i N$, while $\chi_1^{B,IG}$ is invariant under shifts by multiples of $6\pi i T$, i.e., $\hat{\mu}_B \rightarrow \hat{\mu}_B + 6\pi i N$, where N is an arbitrary integer. The periodicity of $\chi_1^{B,SB}$ is a consequence of the Roberge-Weiss symmetry [39], which implies that only states with an integer net baryon number contribute to the partition function. Likewise, the $6\pi i$ periodicity of $\chi_1^{B,IG}$ is a consequence of the states with fractional baryon number accessible in a gas of noninteracting quarks.

Closely related to the periodicity of $\chi_1^{B,SB}$ and $\chi_1^{B,IG}$ is the location of singularities in the complex $\hat{\mu}_B$ plane. Both $\mathrm{Li}_n(z)$ and $\log(1 - z)$ have branch points at $z = 1$. Hence, the singularities of $\chi_1^{B,SB}$ closest to $\hat{\mu}_B = 0$ are located on the imaginary axis, at $\hat{\mu}_B = \pm i\pi$. On the other hand, the closest singularities of the ideal quark gas, $\chi_1^{B,IG}$, are found at $\hat{\mu}_B = \pm 3i\pi$. We note that the latter is generated by the pole of the Fermi-Dirac function at $\hat{p} = 0$. For nonzero quark mass m, these thermal branch points are shifted away from the imaginary axis to $\hat{\mu}_B = \pm\hat{m} \pm 3i\pi$, where $\hat{m} = m/T$.

Thus, the singularity structure of the net baryon density is, in the Stefan-Boltzmann limit, completely determined by the analytic properties of the polylogarithm. In the following, we show that this is the case also for the CEM.

We first note that the Fourier coefficients of the baryon density in Eq. (3) can be expressed in the following form:

$$b_k^{\mathrm{CEM}}(T) = c\lambda^k b_k^{SB} \qquad (16)$$

where

$$c(T) = \left[\frac{b_1(T)}{b_1^{\mathrm{SB}}}\right]^2 \frac{b_2^{\mathrm{SB}}}{b_2(T)}, \qquad (17)$$

$$\lambda(T) = \frac{b_1^{\mathrm{SB}}}{b_1(T)} \frac{b_2(T)}{b_2^{\mathrm{SB}}}. \qquad (18)$$

Also in this case, a closed-form expression for the density can be obtained by resumming the Fourier series,

$$\begin{aligned}
\chi_1^{B,\mathrm{CEM}} &= c\sum_{k=1}^{\infty} \lambda^k b_k^{CEM} \sinh(k\hat{\mu}_B) \\
&= \frac{2c}{27\pi^2}\sum_{s=\pm1} s\left[\sum_{k=1}^{\infty}\frac{3(-\lambda e^{-s\hat{\mu}_B})^k}{k^3} + 4\pi^2\sum_{k=1}^{\infty}\frac{(-\lambda e^{-s\hat{\mu}_B})^k}{k}\right] \\
&= \frac{2c}{27\pi^2}\sum_{s=\pm1} s[3\mathrm{Li}_3(-\lambda e^{-s\hat{\mu}_B}) - 4\pi^2\log(1+\lambda e^{-s\hat{\mu}_B})].
\end{aligned}$$
$$(19)$$

Now, just as in the Stefan-Boltzmann limit [Eq. (12)], the singularity structure of $\chi_1^{B,\mathrm{CEM}}$ can be readily deduced using the analytic properties of the polylogarithms. The two expressions differ only in the prefactor $c(T)$ and the fugacity parameter $\lambda(T)$. The latter, being less than unity, shifts the location of the branch cuts away from the imaginary $\hat{\mu}_B$ axis, into the complex $\hat{\mu}_B$ plane. Thus, the singularities nearest to $\hat{\mu}_B = 0$ are located at $\hat{\mu}_B = \pm \log \lambda \pm i\pi$. This closely resembles the effect of a nonzero quark mass on the thermal branch points.

The radius of convergence of a Taylor expansion about $\mu_B = 0$ is given by the distance to the closest singularity,

$$R = \sqrt{(\log \lambda(T))^2 + \pi^2}. \qquad (20)$$

In Fig. 4 we show $R(T)$ computed using the Fourier coefficients obtained in LQCD as input. The results obtained with Eqs. (20) and (18) for each lattice point coincide with those obtained in Ref. [41] by summing the Fourier series numerically and using the Mercer-Roberts estimator [42] of the radius of convergence. It is thus clear that the CEM does not contain information on singularities in the chemical potential plane with $|\mathrm{Im}\hat{\mu}| < \pi$. In other words, the CEM exhibits only the singularities of Eq. (19), which are associated with the periodicity in the imaginary part of the baryon chemical potential.

Similarly, the Fourier series of the RFM can be also resummed and expressed by the polylogarithm functions. Consequently, neither CEM nor RFM can provide any insight into the location of the chiral transition or the existence of the QCD critical point. However, phenomenological models like CEM can be used as a useful parametrization of noncritical quantities in QCD.

As we discuss in the following section, criticality is reflected in characteristic properties of high-order Fourier coefficients, which are not reproduced by the CEM or RFM.
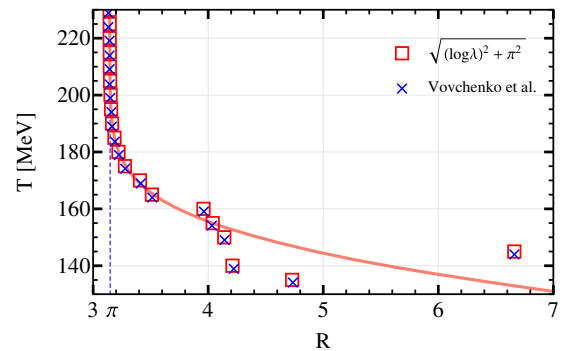

FIG. 4. The radius of convergence computed numerically in Ref. [41] and the distance of the nearest singularity of the polylogarithm to the origin (20). The solid curve was obtained using the fitted values (11) for b_1 and b_2, as explained in the text.

III. FOURIER COEFFICIENTS IN A QCD-LIKE EFFECTIVE MODEL

In the previous section, we have demonstrated that the Fourier coefficients b_k cannot be fixed uniquely by knowledge of the first few. In this section we explicitly examine the effects of critical behavior on the Fourier coefficients within a QCD-like chiral effective model. For this purpose we employ the two-flavor Polyakov-loop quark-meson model [5,37], which captures characteristics of QCD at imaginary baryon chemical potential [38].

A. Criticality in the PQM model

In the PQM model, the thermodynamic potential at nonvanishing temperature T and imaginary quark chemical potential $\theta_q = \mathrm{Im}\mu_q/T$ exhibits the Roberge-Weiss periodicity [39], a residual of the $Z(N_c)$ symmetry, which is an exact symmetry of QCD in the limit of infinitely heavy quarks. The Polyakov–Nambu–Jona-Lasinio model [43,44] is expected to yield compatible results, since the phase structures, including the Roberge-Weiss transition, are very similar in the two models [45,46].

In the following we adopt the mean-field approximation, including renormalized quark vacuum fluctuations [47]. The thermodynamic potential per unit volume Ω in the PQM model is obtained by extremizing the functional

$$\Omega(\sigma, \Phi, \Phi^*) = \mathcal{U}(\Phi, \Phi^*) + U(\sigma) + \Omega_{q\bar{q}}(\sigma, \Phi, \Phi^*) \quad (21)$$

with respect to the thermal expectation values of the Polyakov loop Φ, its conjugate Φ^*, and the sigma field σ. Here $\mathcal{U}(\Phi, \Phi^*)$ and $U(\sigma)$ are the Polyakov loop potential and the purely mesonic potential for the $O(4)$ multiplet $(\sigma, \vec{\pi})$, while $\Omega_{q\bar{q}}$ denotes the quark contribution to the thermodynamic potential. We employ the polynomial form for $\mathcal{U}$ [44],

$$\frac{\mathcal{U}(\Phi, \Phi^*)}{T^4} = -\frac{u_2(T)}{2}\Phi^*\Phi - \frac{u_3}{6}(\Phi^3 + \Phi^{*3}) + \frac{u_4}{4}(\Phi^*\Phi)^2, \quad (22)$$

with

$$u_2(T) = a_0 + a_1\left(\frac{T_0}{T}\right) + a_2\left(\frac{T_0}{T}\right)^2 + a_3\left(\frac{T_0}{T}\right)^3. \quad (23)$$

The parameters in the potential are adjusted so as to reproduce the equation of state of the pure gluonic matter with $u_3 = 0.75$, $u_4 = 7.5$, $a_0 = 6.75$, $a_1 = -1.95$, $a_2 = 2.625$, $a_3 = -7.44$, and $T_0 = 270$ MeV. The mesonic potential is given by

$$U(\sigma) = \frac{\lambda}{4}(\sigma^2 - v^2)^2 - h\sigma \quad (24)$$

where the pion field is suppressed, since we do not consider pion condensation. The explicit chiral symmetry breaking parameter equals $h = f_\pi m_\pi^2$.

The quark contribution consists of a vacuum fluctuation part and a purely thermal part,

$$\Omega_{q\bar{q}}(\sigma, \Phi, \Phi^*) = -\frac{N_c N_f}{8\pi^2}m_q^4 \ln\left(\frac{m_q}{M}\right)$$
$$- 2N_f T \int \frac{d^3 p}{(2\pi)^3}\ln(g^+) + \ln(g^-), \quad (25)$$

where M is an arbitrary renormalization scale,

$$g^+(\sigma, \Phi, \Phi^*, T, \mu_q) = 1 + 3\Phi e^{-(E_q - \mu_q)/T}$$
$$+ 3\Phi^* e^{-2(E_q - \mu_q)/T} + e^{-3(E_q - \mu_q)/T} \quad (26)$$

and

$$g^-(\sigma, \Phi, \Phi^*, T, \mu_q) = g^+(\sigma, \Phi^*, \Phi, T, -\mu_q). \quad (27)$$

Here the quark mass and energy are given by $m_q = g\sigma$ and $E_q = \sqrt{p^2 + m^2}$, respectively.

The Polyakov loop variables Φ and Φ^* take real values for real μ_q, such that one can pick $L = |\Phi|$ and $\bar{L} = |\Phi^*|$ as the two independent variables. On the other hand, for imaginary values of the chemical potential they are complex conjugates of each other. Thus, the two independent variables are conveniently chosen as the modulus L and the phase ϕ, $\Phi = Le^{i\phi}$ and $\Phi^* = Le^{-i\phi}$. The expectation values are then determined by the stationarity condition

$$\frac{\partial\Omega}{\partial\sigma} = \frac{\partial\Omega}{\partial L} = \frac{\partial\Omega}{\partial\phi} = 0, \quad (28)$$

and all thermodynamic quantities can be obtained from the thermodynamic potential $\Omega(T, \mu_q)$.

With $N_c = 3$ and $N_f = 2$, the vacuum parameters are fixed to be $f_\pi = 93$ MeV, $m_\pi^{\mathrm{phys}} = 138$ MeV, and $m_\sigma = 600$ MeV, while the Yukawa coupling is set to $g = 3.35$.

In general, the pseudocritical temperature of a crossover transition is not uniquely determined. By maximizing the chiral (χ_σ) and Polyakov loop (χ_L) susceptibilities, we find, at $\mu_q = 0$, the crossover temperatures 231 and 213 MeV for the chiral and deconfinement transitions, respectively. An alternative determination, obtained by maximizing the temperature derivatives of the order parameters, $d\sigma/dT$ and dL/dT, yields 226 and 223 MeV respectively. In the chiral limit the two procedures yield a unique chiral critical temperature.

In the following, we control the strength of the explicit symmetry breaking by varying the pion mass in vacuum
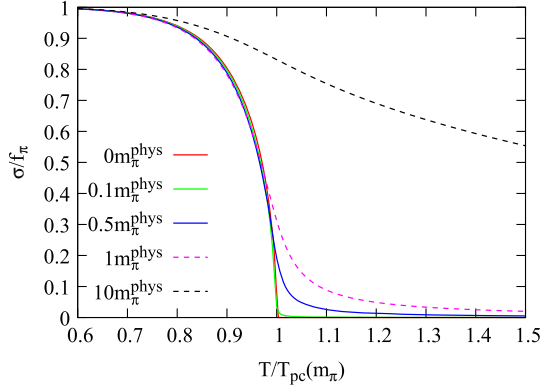
FIG. 5. The chiral order parameter in the PQM model for several values of the pion mass. The temperature is normalized by the (pseudo)critical temperature $T_{pc}(m_\pi)$, for each value of the pion mass. In the chiral limit, $T_{pc}(m_\pi = 0) \equiv T_c$.

from $m_\pi = 0$ (chiral limit) to $m_\pi = 10\, m_\pi^{\text{phys}}$, in order to assess the effect of criticality on the Fourier coefficients. Thereby, we keep the same vacuum values for f_π and m_σ by readjusting the parameters in U_σ. The resulting chiral order parameter at $\mu_B = 0$ is shown in Fig. 5. The chiral critical temperature in the chiral limit is found to be 228.256 MeV. For a finite, but small, pion mass $(0.1 m_\pi^{\text{phys}})$ the pseudocritical temperatures obtained using χ_σ and $d\sigma/dT$ are 229 and 227 MeV, respectively. Hereafter, for simplicity, we denote by T_{pc} the pseudocritical temperature corresponding to a maximum of χ_σ. However, in the heavy pion mass case, the chiral pseudocritical temperature[2] $T_{pc} = 228$ MeV is determined by the maximum of $d\sigma/dT$.

The behavior of order parameters and the phase structure in the chiral effective models have been investigated in Refs. [38,46,48]. For the present study we summarize a few relevant features. In Fig. 6, we show contour maps for the temperature derivative of the chiral order parameter $d(\sigma/f_\pi)/dT$ in the plane of imaginary chemical potential vs temperature in the chiral limit and for two nonzero values of the pion mass.

In the left panel of Fig. 6, one can unambiguously identify the chiral critical line in the chiral limit, which extends to higher temperature at large θ_B, and merges with the Roberge-Weiss transition line at $\theta_B = \pi$ at the critical temperature $T_c(\theta_B = \pi) = 311$ MeV. This first-order transition line extends from $T = \infty$ down to the so-called Roberge-Weiss end point, which exhibits a second-order phase transition at $(T = T_{\text{RW}}, \theta_B = \pi)$. We find $T_{\text{RW}} = 308.1$ MeV $= 1.35 T_c$ which is slightly below $T_c(\theta_B = \pi)$. At $T > T_{\text{RW}}$, the thermodynamic quantities resemble qualitatively those of a Stefan-Boltzmann gas.

In the case of a nonvanishing pion mass (the middle and the right panel in Fig. 6), the rapid change of the order parameter found for a small pion mass is smoothed, such that the region around the maximum indicates the location of the crossover transition. Moreover, we find that the curvature of the pseudocritical line is reduced at small θ_B as the pion mass is increased.

In LQCD calculations, it is found that the nature of the Roberge-Weiss end point depends on the quark mass [49,50]. Thus, for small quark masses it is a triple point (the junction of three first-order phase transitions), while at intermediate values of the quark mass, it is a $Z(2)$ critical point. Finally, for large quark masses, the RW end point is again a triple point. In the model considered here, the RW end point is located at $T_{\text{RW}} = 311$ MeV $\simeq 1.35 T_{pc}$ and 327 MeV $\simeq 1.43 T_{pc}$ for the physical and heavy values of the pion mass, respectively, and is second order in both cases.[3]

Given the phase structure in the plane of imaginary chemical potential vs temperature, shown in Fig. 6, one expects that the Fourier coefficients b_k at intermediate temperatures, $T_{pc} \leq T \leq T_{\text{RW}}$, reflect the existence of the transition line.

B. The Fourier coefficients in the chiral limit

In order to identify the influence of criticality on the Fourier coefficients, we first consider the PQM model formulated in the chiral limit. The expansion coefficients b_k are computed by Fourier transforming the density as a function of the imaginary chemical potential, as in Eq. (9). The numerical procedure applied to compute b_k was tested on the Stefan-Boltzmann gas, and the results are found to be accurate for Fourier coefficients b_k on the order of $\sim 10^{-9}$ or larger. We note that the applicability of the procedure is limited by the magnitude of the coefficients rather than their order k.

In Fig. 7 we show the normalized baryon density $\text{Im}\chi_1^B$ in the PQM model calculated in the chiral limit at imaginary chemical potential and at several temperatures near T_c. The solid lines represent the density obtained directly from the PQM thermodynamic potential by differentiating with respect to the chemical potential, $\chi_1^B = \partial(p/T^4)/\partial\hat{\mu}_B$. Also shown are the densities reconstructed from the Fourier coefficients obtained in the PQM model using Eq. (2). Finally, we also show the reconstructed densities obtained by using the CEM ansatz (3) applied to the PQM model.

At $T = T_c$, the densities coincide, as is expected from the smooth behavior of the density. However, at $T/T_c = 1.2$ (blue solid curve), the chiral phase boundary, shown in Fig. 7, appears as a kink at $\theta_B/\pi \simeq 0.88$. While the kink is reproduced by the density reconstructed from the Fourier

---

[2]In this particular case, χ_σ yields an unusually small transition temperature owing to the sigma-meson mass being much lighter than that of the pion.

[3]See also Ref. [46], where different forms of the Polyakov loop potential $\mathcal{U}(\Phi, \Phi^*)$ were explored.
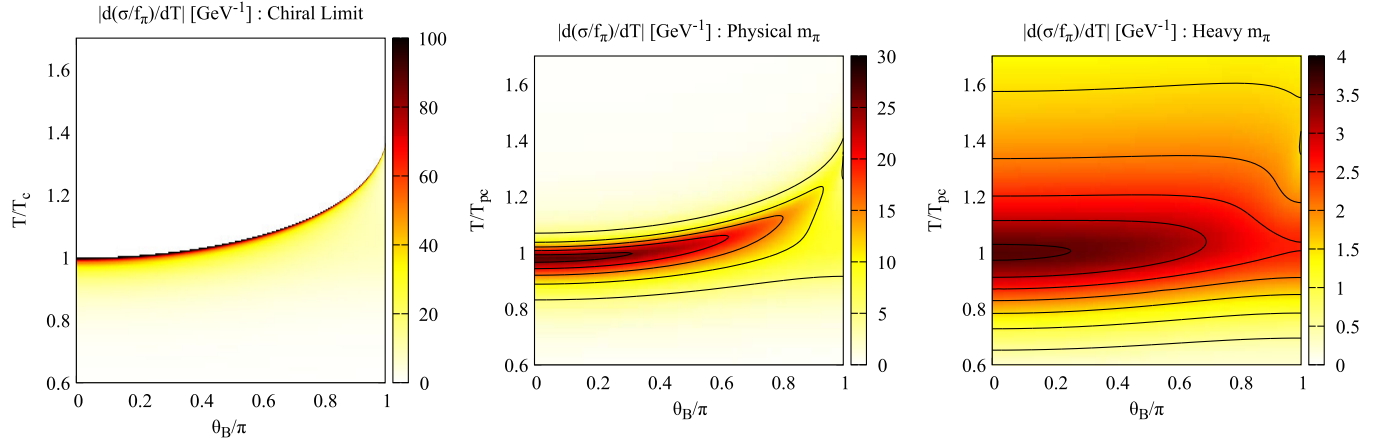
FIG. 6.   Contour maps for $d(\sigma/f_\pi)/dT$ in the $T - \theta_B$ plane. The left, middle and right panels correspond to the vanishing, physical and heavy pion mass cases, respectively.
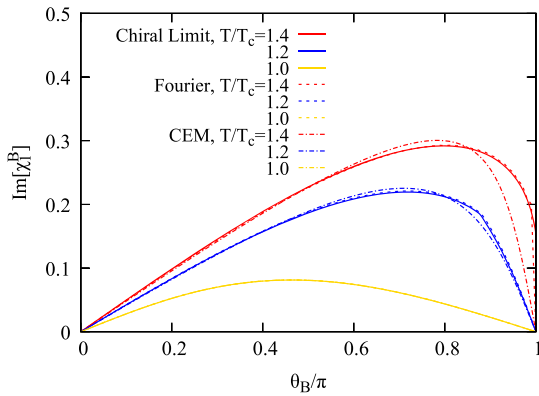

FIG. 7.   The imaginary part of the baryon density at imaginary chemical potential in the chiral limit. Solid lines are obtained by differentiating the pressure with respect to $\hat{\mu}_B$. The dashed lines represent the density reconstructed from the Fourier series and the dashed-dotted lines denote the density reconstructed from the Fourier coefficients obtained using the CEM ansatz.

coefficients, the CEM ansatz yields a smooth, analytic function. This is expected, since the CEM Fourier coefficients do not capture the power-law behavior of the higher-order coefficients, which is needed to reproduce the singularity.

At $T/T_c = 1.4$, the density does not vanish at $\theta_B = \pi$. This, together with the fact that the density is an odd function of θ_B that exhibits the Roberge-Weiss periodicity, implies that it must be discontinuous at this point. The discontinuity is a manifestation of the first-order Roberge-Weiss transition [39].

Since $\sin(k\theta_B)$ vanishes at $\theta_B = \pi$ for any integer k, the density reconstructed from a finite number of terms in the Fourier series (2) must also vanish at $\theta_B = \pi$. We note that the density reconstructed from the CEM coefficients shows a stronger deviation near $\theta_B = \pi$. Moreover, even the closed form expression (19) for the resummed CEM

Fourier series does not reproduce the discontinuity in the density for $\lambda < 1$, i.e., $T < \infty$. Thus, we expect significant differences between high-order b_k and b_k^{CEM} at temperatures beyond T_{RW}. In the following, we explore the structure of the Fourier coefficients b_k in more detail.

At temperatures significantly below T_c, the PQM model exhibits statistical confinement. Consequently there is an oscillatory dependence of the thermodynamic potential on the imaginary baryon chemical potential, with $\Delta\Omega(T, \theta) \sim \cos(3\theta_q) = \cos\theta_B$ [46], as in the hadron resonance gas. Therefore the density is, to a good approximation, that of a classical Boltzmann gas, $\text{Im}\chi_1^B \sim \sin\theta_B$, with small corrections from quantum statistics and interactions. This, in turn, implies that the higher-order Fourier coefficients are strongly suppressed, as in the CEM. Our results confirm this expectation up to $T/T_c \leq 0.9$ for Fourier coefficients of order $k < 9$. Owing to the numerical limitations mentioned above, coefficients of higher order, i.e., $k \gtrsim 10$, cannot be computed reliably in this temperature range, within the present scheme.

Given the results on the signature of the Roberge-Weiss transition in the Fourier series, one may expect that the chiral critical line at real values of the baryon chemical potential [51–53] could also contribute significantly to the high-order Fourier coefficients. However, contributions to the Fourier coefficients from singularities located at real μ_B are exponentially suppressed [36], i.e., $\Delta b_k \sim e^{-k|\text{Re}\hat{\mu}_B|}$. This leads to an exponential suppression also of the contribution from the thermal branch points discussed in Sec. II B for nonzero fermion masses, with $\Delta b_k \sim e^{-km}$.

From general scaling considerations one finds that at $T = T_c$ and at large k, mean-field criticality leads to an asymptotic dependence of $b_k \sim 1/k^4$ [36]. However, since in this case the integration contour, except for the point $\theta_B = 0$, lies in the chirally broken phase, a major contribution to the Fourier coefficients is due to massive fermion degrees of freedom. Consequently, the initial
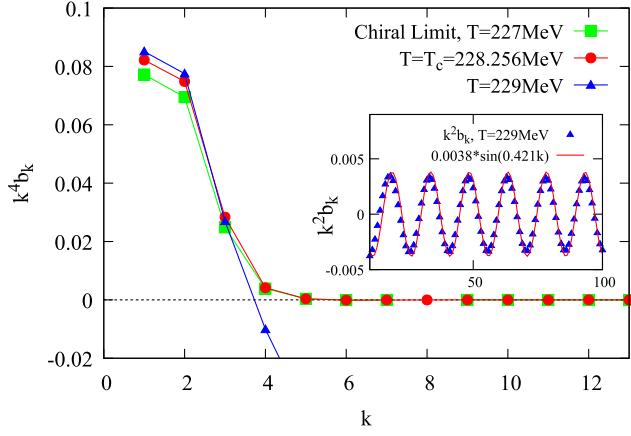
FIG. 8.   Fourier coefficients $k^4 b_k$ in the chiral limit at temperatures near T_c. The inset shows $k^2 b_k$ at a temperature slightly above T_c, $T = 229$ MeV. The solid line represents a fit with $A\sin(k\theta_c)$, as discussed in the text.

k-dependence of the Fourier coefficients is exponential, while the contribution of the critical point θ_B is fairly small, implying that the power law is visible only at very large k.

Figure 8 shows b_k around $T = T_c = 228.256$ MeV. Here we have multiplied b_k by k^4 in order to highlight the large k behavior of the Fourier coefficients. One observes a rapid suppression of b_k with increasing order below and at T_c, in line with a substantial contribution of massive degrees of freedom to the baryon density. Thus, at temperatures $T \le T_c$, the density is saturated by the first few Fourier coefficients. Consequently, the CEM ansatz is able to reproduce the baryon density at $T = T_c$, as shown in Fig. 7, although the model does not yield the correct asymptotic behavior of the Fourier coefficients. Moreover, owing to the dominant contribution of massive degrees of freedom, it is extremely difficult, if not impossible, to reliably extract the asymptotic $1/k^4$ behavior of the coefficients in numerical calculations.

At a temperature slightly above T_c, we find that b_k exhibits oscillations, with a $1/k^2$ dependence superimposed, as shown in the inset in Fig. 8 for $T = 229$ MeV. This characteristic dependence on k is expected at temperatures between the critical temperature at $\mu_B = 0$, T_c, and the Roberge-Weiss temperature T_{RW}. In this temperature range, the critical point is located on the imaginary μ axis (see Fig. 10). It follows that the Fourier coefficients take the asymptotic form $A\sin(k\theta_c)/k^2$ [36], where $\theta_c = \mathrm{Im}\mu_c/T$ is the critical value of the baryon chemical potential. Indeed, a fit of the oscillatory dependence on k shown in Fig. 8 yields $\theta_c = 0.421$, in perfect agreement with the location of the critical point at $T = 229$ MeV.

The expectation that the oscillation frequency depends on the location of the singularity is confirmed by the behavior of b_k at higher temperatures. In Fig. 9 we show the Fourier coefficients at $T/T_c = 1.1$, 1.2, and 1.3. Here we
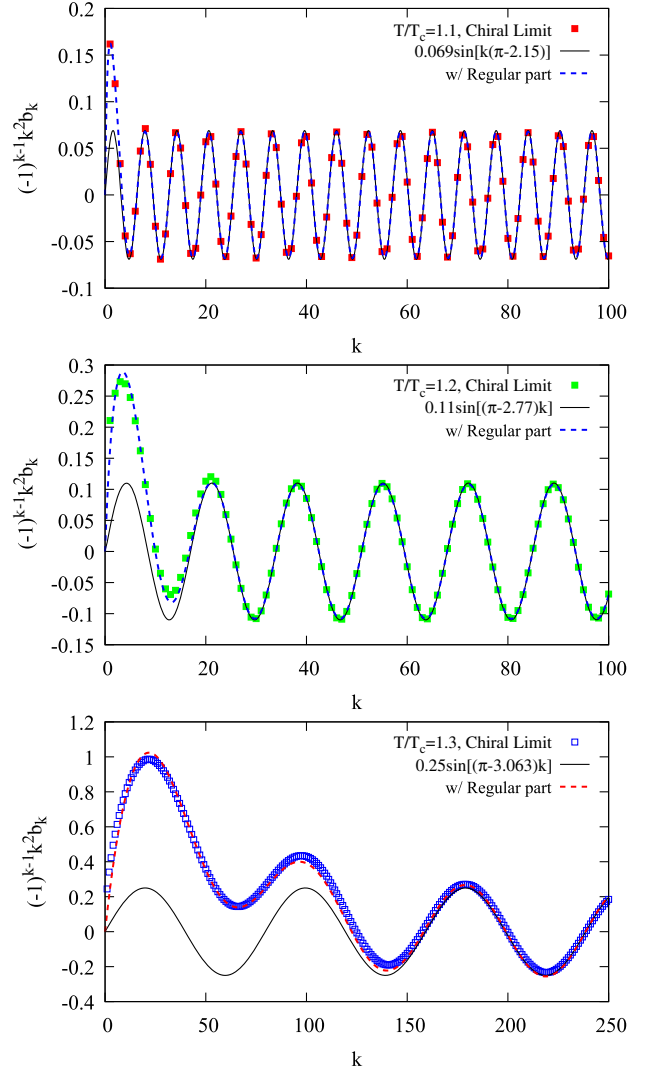

FIG. 9.   Fourier coefficients of the PQM model in the chiral limit at $T/T_c = 1.1$ (top), 1.2 (middle), and 1.3 (bottom). The solid lines show a fit with $A\sin[(\pi - \theta_c)k]$.

have multiplied b_k by $(-1)^{k-1}$. The additional phase changes the frequency of the oscillation from θ_c to $\pi - \theta_c$ and thus yields oscillations that are more easily discernible. This is because it is difficult to identify a frequency larger than $\pi/2$ on the discrete k grid. The lines show fits with the functional form $A\sin[k(\pi - \theta_c)]$. Also shown in Fig. 9 are fits where a contribution of the regular part of the baryon density, outside the critical region, is included: $CK_2(ak)/k + A\sin[k(\pi - \theta_c)]$. Here $K_2(x)$ denotes the modified Bessel function of the second kind. The values obtained for $\theta_c = 2.15$, 2.77, and 3.063 are in agreement with the location of the chiral critical point for the corresponding temperature. For instance, $\theta_c = 2.77$ at $T/T_c = 1.2$ yields $\theta_c/\pi = 0.88$, which is the position of the kink in the density in Fig. 7.

The increase of θ_c with temperature is a consequence of the shape of the phase boundary (see Fig. 6), which shifts to

larger values of θ with increasing temperature. We conclude that the high-order Fourier coefficients carry information on the chiral phase transition at imaginary values of the baryon chemical potential.

C. Fourier coefficients at nonzero pion masses

For nonzero pion masses, the chiral symmetry is explicitly broken, implying that the chiral transition is of the crossover type and that the analytic properties of the baryon density in the complex chemical potential plane are modified. Specifically, there is a shift of the chiral critical point from the real or imaginary axis into the complex chemical potential plane [52,53], as illustrated in Fig. 10. Owing to the real part of the chemical potential at the singularity, the high-order Fourier coefficients exhibit exponential damping in addition to the power-law scaling and oscillatory behavior found in the chiral limit for temperatures above T_{pc} [36].

The resulting Fourier coefficients for temperatures near the crossover temperature T_{pc} are shown in Fig. 11. The upper panel shows the results for a small pion mass, $m_\pi = 0.1 m_\pi^{\mathrm{phys}}$. At $T = T_{pc}$, we find an oscillatory behavior of $k^4 b_k$, accompanied with a slow damping of the amplitude. A comparison with temperatures slightly above and below T_{pc} shows that the oscillation frequency increases with temperature, while the damping of the amplitude is reduced with temperature. This observation is in qualitative agreement with the temperature dependence of the location of the singularity in the complex chemical potential plane, shown schematically in Fig. 10.

We note that, given the limited range in k available ($k \lesssim 50$), one cannot distinguish between a fit with a function proportional to e^{-ak}/k^2 with large a from one proportional to e^{-ak}/k^4 and small a. Nevertheless, these results clearly demonstrate the sensitivity of the Fourier coefficients to small changes in temperature and pion mass and thus to chiral criticality.

In the lower panel of Fig. 11, we show the Fourier coefficients for a somewhat heavier pion mass, equal to $0.5 m_\pi^{\mathrm{phys}}$. Here the temperature dependence of the oscillation frequency is reduced. This is expected, since the relevant energy scale, the pion mass, is now large compared to the few MeV change in the temperature. Nevertheless, the qualitative behavior of the oscillations as a function of temperature is still consistent with the expected motion of the singularity in the complex chemical potential plane. Thus, the frequency increases and the damping of the amplitude weakens with increasing temperature.

Unlike the critical temperature in the chiral limit, the pseudocritical temperature T_{pc} is not clearly distinguished by a sudden change in the properties of the Fourier components b_k. This is a rather natural consequence of the shift of the singularity into the complex chemical potential plane, indicated in Fig. 10. As the temperature
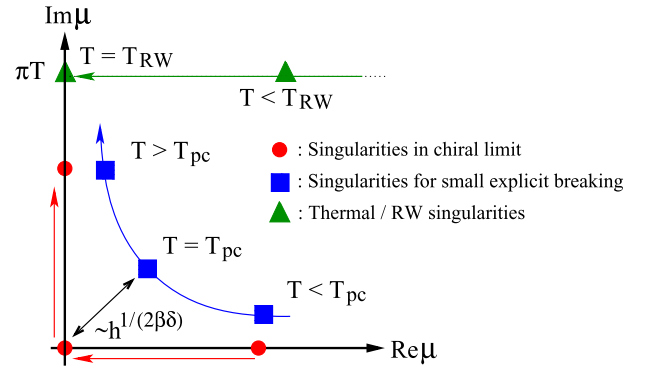

FIG. 10. Schematic view of the singularities in the complex chemical potential plane (first quadrant only). The arrows indicate the direction each singularity moves when the temperature is increased.

is increased and passes T_{pc}, the motion of the singularity in the complex plane leads to a slow increase of the oscillation frequency and a smooth reduction of the exponential damping of the amplitude.
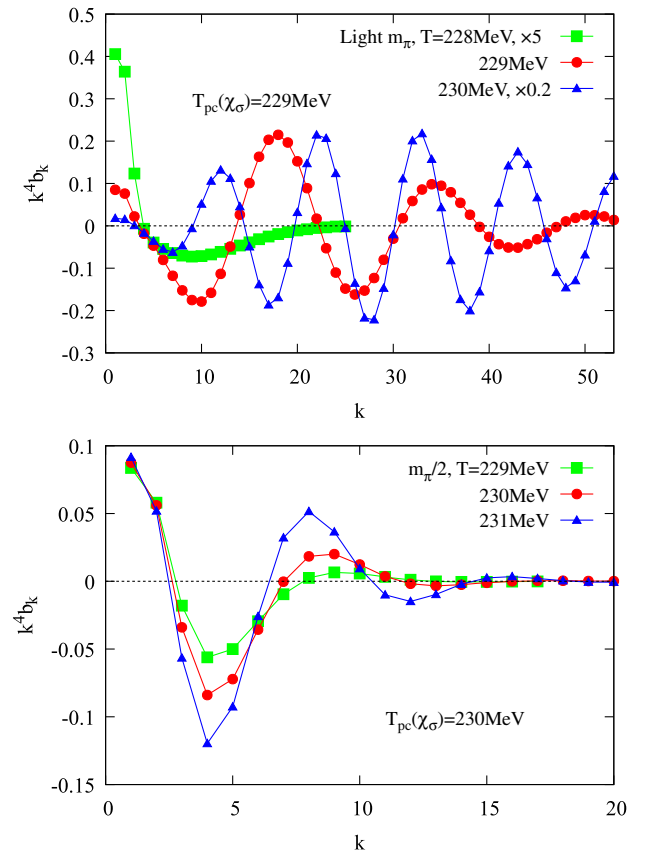

FIG. 11. The Fourier coefficients $k^4 b_k$ at $m_\pi = 0.1 m_\pi^{\mathrm{physical}}$ (upper panel) and at $0.5 m_\pi^{\mathrm{phys}}$ (lower panel) for temperatures near T_{pc}. In the lower panel, the results at $T = 228$ and 229 MeV have been multiplied by the factors 5 and 0.2, respectively.
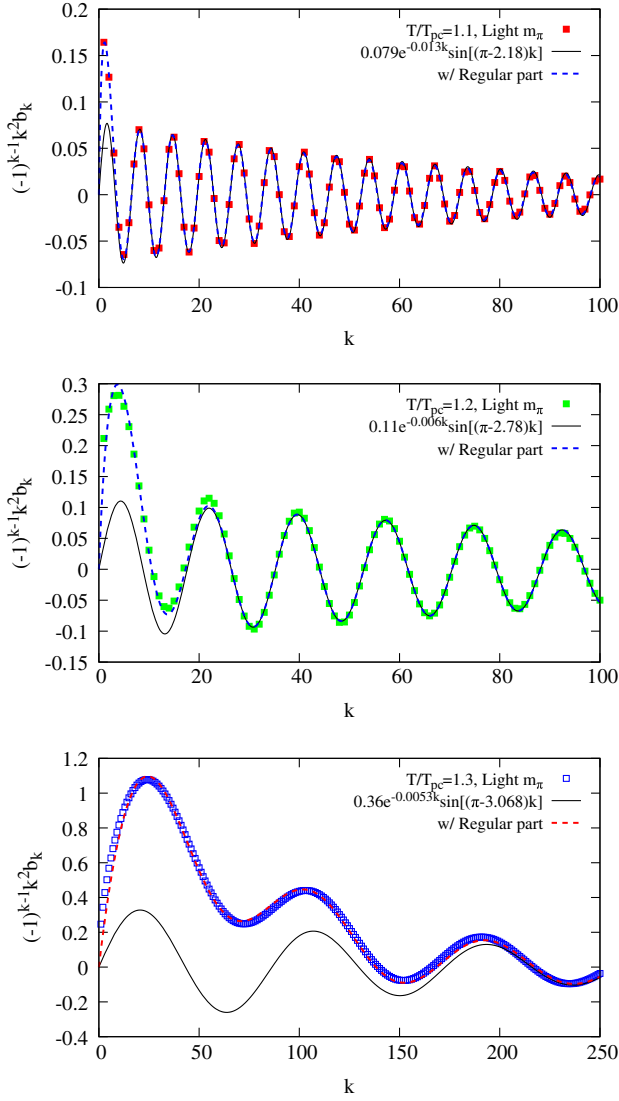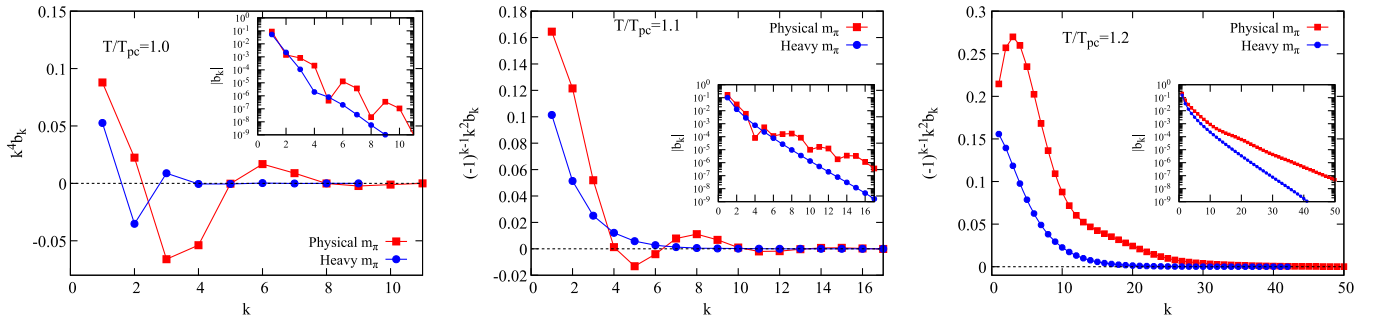
FIG. 12.   Same as Fig. 9, but for the light pion mass.

As in Fig. 9, we show in Fig. 12 the Fourier coefficients multiplied by the factor $(-1)^{k-1}k^2$ at $T/T_{pc} = 1.1$, 1.2, and 1.3. In order to fit the large k dependence of the coefficients b_k, we introduce an exponential damping factor of the form

e^{-ak}, as well as a regular part. The temperature dependence of the oscillation frequency and the damping factor is again consistent with the expectations deduced from Fig. 10.

A comparison of the results for small pion masses with those obtained in the chiral limit shows that the higher-order Fourier coefficients are exponentially damped by the explicit breaking of chiral symmetry. Therefore, it is a quantitative question whether chiral criticality can be identified in the Fourier coefficients also for larger pion masses. In order to address this issue, we present the Fourier coefficients obtained in the PQM model for the physical and for a heavy pion mass in Fig. 13.

As illustrated in Fig. 5, in the mean-field approximation the PQM model exhibits a rather rapid chiral crossover transition for a pion mass equal to the physical one, while LQCD yields a smoother transition at the physical point [54,55]. Therefore, a mean-field calculation with a larger pion mass, somewhere between the physical and the heavy pion mass employed here, may be more relevant for a comparison with lattice results.

In the left panel of Fig. 13 we show $k^4 b_k$ for physical (squares) and heavy (circles) pion masses at $T = T_{pc}$. For a physical pion mass, the behavior is qualitatively similar to that shown in the lower panel of Fig. 11.

We note that the sign structure of the Fourier coefficients differs from the alternating signs of the LQCD results (see Fig. 1 and Ref. [40]). As indicated above, the oscillation frequency depends on the location of the contributing singularities in the complex chemical potential plane, in particular on their imaginary parts, as well as on the strength of the individual contributions. Thus, the sign structure of the Fourier components is determined by an interplay between the chiral singularity and, e.g., the thermal branch point. Consequently, the staggered sign structure seen in the LQCD results at $T = T_{pc}$ may be due to noncritical physics, not captured by the PQM model.

The oscillations lead to deviations from a pure exponential damping of the magnitude of the Fourier coefficients, as shown in the inset of the left panel of Fig. 13, while for the heavy pion mass, the oscillations are almost completely washed out by the strong damping.

FIG. 13.   The Fourier coefficients b_k for physical and heavy pion masses in the PQM model. From left to right, the results are shown for $T/T_{pc} = 1.0$, 1.1, and 1.2, respectively. The insets show the magnitude of $|b_k|$ on a logarithmic scale.

In the middle and center panels of Fig. 13 we show $(-1)^{k-1}k^2 b_k$ at $T/T_{pc} = 1.1$ and 1.2. The additional phase factor compared to the left panel removes the dominant oscillation to a large extent and hence yields clearer plots. At $1.1T_{pc}$, almost all points are at positive values, with a few exceptions for the physical pion mass. Moreover, at $1.2T_{pc}$ the sign changes are completely removed by the phase factor. This implies that the staggered sign structure of the LQCD results on the first four Fourier coefficients [40] is reproduced at temperatures somewhat above the pseudocritical temperature T_{pc}.

As shown in the insets in the middle and right panels, we indeed find an exponential damping of the magnitude of b_k for the heavy pion mass for k larger than 3 or 4. At $T = 1.2T_{pc}$, a small amplitude, low-frequency residual oscillation, left after removing the dominant one with the phase factor $(-1)^{k-1}$, would be difficult to recognize, owing to the fast exponential damping. Nevertheless, the shoulder around $k \sim 10\text{--}20$ for the physical pion mass (see inset) may be the signature of such an oscillation.

From the above discussion, it is clear that the location of the singularity associated with the chiral transition in the complex chemical potential plane is reflected in characteristic k-dependencies of the Fourier coefficients b_k. However, the presence of other singularities, which interfere with the chiral one, and the exponential damping of the Fourier coefficients for physical pion masses make the analysis less clear cut.

D. The effect of the Roberge-Weiss transition on the Fourier coefficients

Irrespective of the value of the pion mass, the Roberge-Weiss transition appears at $T \geq T_{RW}$. It is a first-order transition, which ends at $T = T_{RW}$. Assuming that the RW end point is a second-order critical point, one finds that the leading contribution to the high-order Fourier coefficients at $T = T_{RW}$ is of the form $b_k \sim (-1)^{k-1}k^{-(1+1/\delta)}$ [36], where δ is the critical exponent associated with the external field strength in the $Z(2)$ universality class. In Fig. 14 we show the Fourier coefficients at $T = T_{RW}$ for the physical value of the pion mass. We find that the coefficients b_k indeed follow a power-law decay with the exponent $4/3$, consistent with $\delta = 3$ in the mean-field approximation. In order to illustrate the sensitivity, we also display b_k at T slightly below and slightly above T_{RW}. The inset shows that the deviation from the $k^{-4/3}$ behavior at the slightly different temperatures is substantial for $k > 10$. We also note that, in the chiral limit, we find a deviation from the $k^{-4/3}$ scaling. We attribute this to the contribution from the chiral phase boundary, which is located close to the RW end point.

At temperatures above T_{RW}, the density is discontinuous at $\theta_B = \pi$, implying that the Fourier coefficients take the asymptotic form [36] $b_k \sim (-1)^{k-1}/k$. This is confirmed by
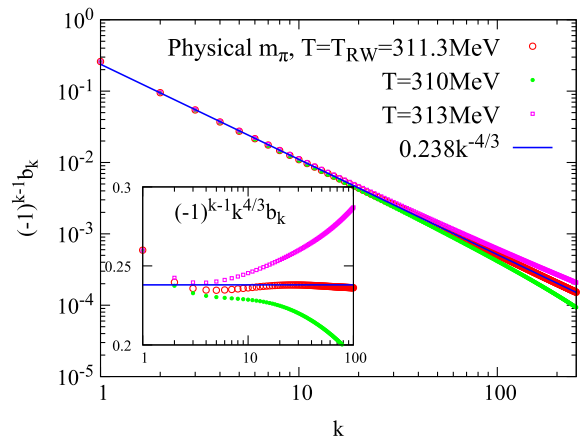

FIG. 14. Fourier coefficients near $T = T_{RW}$ for the physical pion mass. In the inset the coefficients multiplied by $k^{4/3}$ are shown.

Fig. 15, where we plot $|kb_k|$ for $T/T_{pc} = 1.5$. The asymptotic value of kb_k is given by $(2/\pi)\text{Im}\chi_1^B(T, i\pi)$ and thus directly connected with the discontinuity in the density at the Roberge-Weiss transition [36].

For comparison we also show the Fourier coefficients obtained using the CEM scheme in Fig. 15. Clearly, the CEM ansatz does not reproduce the asymptotic behavior of the coefficients related with the RW transition, as anticipated in the discussion of Fig. 7, in Sec. III B. Thus, the CEM ansatz cannot account for the Roberge-Weiss transition, irrespective of the value of the pion mass.

Although these results are obtained in a particular model, the qualitative features are of more general validity, since they are directly linked to the Roberge-Weiss transition.

E. Temperature dependence of low-order coefficients

A crossover or a true phase transition may also be signaled by the temperature dependence of the Fourier
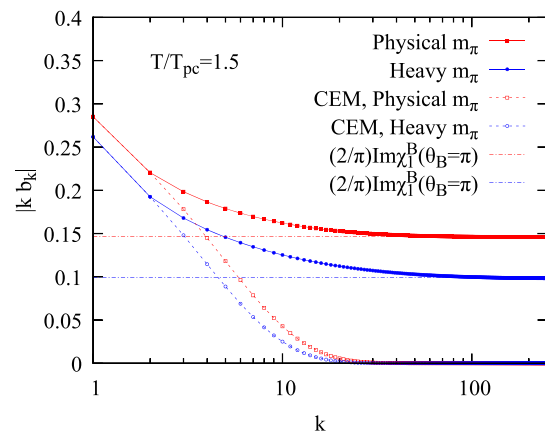

FIG. 15. The Fourier coefficients $|b_k|$ for a temperature above T_{RW} calculated in the PQM model and in CEM. The dashed-dotted horizontal lines indicate the expected asymptotic value, which is determined by the discontinuity in the density.
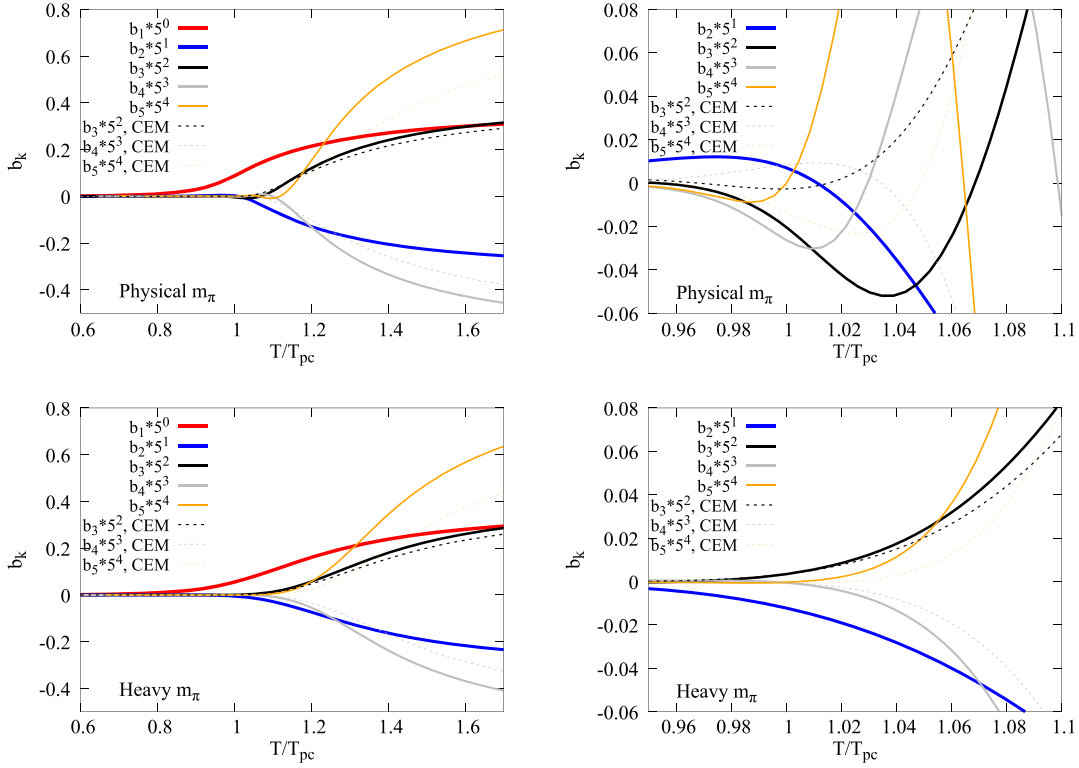
FIG. 16.   The Fourier coefficients b_k in the PQM model as functions of temperature. Solid lines show the PQM model results, while the dashed lines are constructed using the CEM ansatz. The upper and lower figures show the physical and heavy pion mass cases, respectively. In order to improve readability, each b_k is multiplied with a factor 5^{k-1}.

coefficients. In Fig. 16 we show the b_k, up to $k = 5$, as functions of temperature for physical and heavy pion masses. For comparison we also show the coefficients obtained using the CEM ansatz.

For the physical pion mass, the chiral crossover transition is reflected already in the lowest-order coefficients through the oscillations of b_k for temperatures near T_{pc}, as shown in the upper right panel. On the other hand, for a heavy pion mass this oscillatory behavior is suppressed, owing to the stronger smoothening. The coefficients obtained using the CEM ansatz do not exhibit any oscillatory behavior and show substantial deviations from the PQM results with increasing temperature.

These results indicate that already at order $k \geq 2$, the Fourier expansion coefficients may exhibit a nontrivial temperature dependence in the crossover region. We note that the Fourier coefficients obtained in LQCD do not seem to oscillate as functions of temperature [40]. However, as discussed in Sec. III C, the interplay between critical and noncritical physics, and consequently the sign structure of the Fourier coefficients, depends on the location and relative strength of the singularities, which may be different in the model and in QCD. Consequently, we expect that oscillations of the Fourier coefficients in the crossover region will appear also in LQCD calculations, when the location of the chiral singularity approaches the origin of

the complex μ-plane, i.e., for pion masses smaller than the physical value (cf. Fig. 10).

F. Reconstructing susceptibilities from b_k

The characteristic behavior of the Fourier coefficients b_k is reflected also in the baryon number fluctuations. Using Eq. (10), the cumulants at $\mu_B = 0$ can be obtained by using the sum

$$\chi_{2n}^B = \sum_{k=1}^{k_{\max}} k^{2n-1} b_k. \qquad (29)$$

Formally the sum should be extended to infinite order but, provided b_k decreases sufficiently fast with k, the series converges and the summation may be truncated at some moderate value $k_{\max}$.

We find that for $n \leq 8$ the baryon number cumulants χ_{2n}^B computed using Eq. (29) reproduce those obtained directly by taking derivatives of the pressure $\chi_n^B = \partial^n (p/T^4)/\partial \hat{\mu}_B^n$ for temperatures up to $T/T_{pc} \leq 1.1$–1.3. For higher temperatures it is numerically difficult to obtain reliable results for the coefficients b_k at sufficiently high order to reach agreement. We note that there is an intrinsic problem in calculating higher-order cumulants using the Fourier expansion at temperatures above T_{RW}, owing to the slow
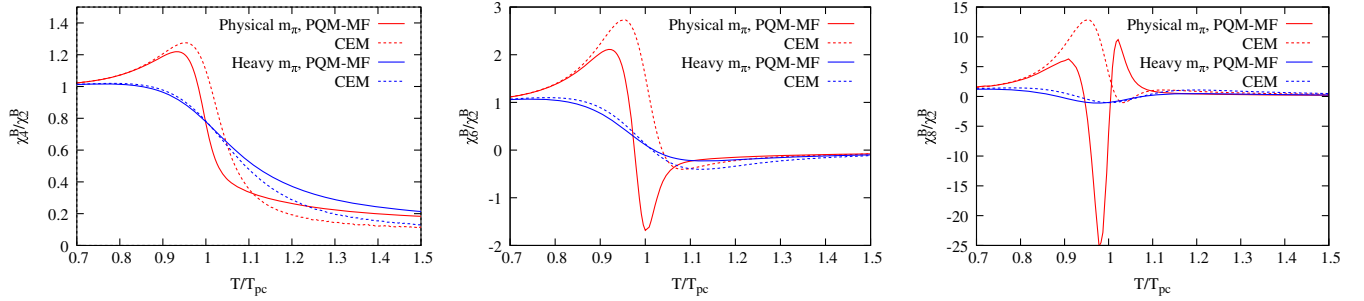
FIG. 17.   The ratio of the fourth- (left), sixth- (middle) and eighth-order (right) baryon number cumulants to the second-order one, calculated in the PQM model and using the CEM ansatz for different pion masses.
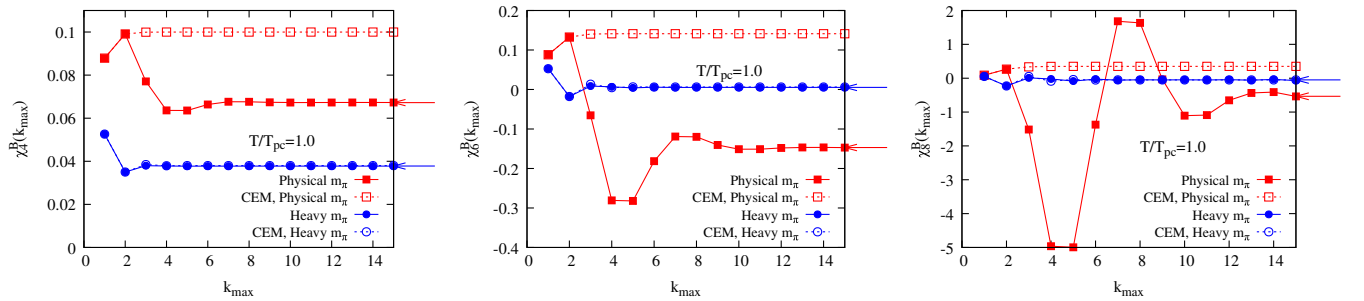

FIG. 18.   Fourth- (left), sixth- (center), and eighth-order (right) cumulants obtained using the partial sum up to $k = k_{max}$ [see Eq. (29)] in the PQM model and adopting the CEM ansatz at $T = T_{pc}$. The arrows indicate the values of the cumulants obtained by taking derivatives of the pressure.

decrease of the b_k with k, which is related to the discontinuity in density at the RW transition.

We first compare the cumulant ratios obtained using the CEM scheme to those computed directly from derivatives of the pressure. In the CEM scheme the summation in Eq. (29) converges, due to the exponential damping of higher-order terms.

Figure 17 displays the χ_4^B/χ_2^B, χ_6^B/χ_2^B, and χ_8^B/χ_2^B cumulant ratios. As expected from the comparison of Fourier coefficients, these cumulant ratios are rather well reproduced in the CEM scheme for a heavy pion mass, where criticality is strongly suppressed. However, for a physical value of the pion mass, the CEM scheme does not reproduce the χ_6^B/χ_2^B and χ_8^B/χ_2^B cumulant ratios,[4] which are sensitive probes of the chiral crossover transition [15]. Although the CEM scheme roughly reproduces the sign structure of the cumulant ratios, it clearly fails to capture the location of sign changes and the magnitude of the fluctuations.

The reason for these differences between the cumulants of the PQM model and those obtained in the CEM scheme can be traced back to the asymptotic behavior of the Fourier coefficients. In Fig. 18 we show the higher-order cumulants computed at $T = T_{pc}$. Since each derivative with respect to the chemical potential brings one power of k in Eq. (29), the higher-order cumulants are more sensitive to the higher-order coefficients.[5]

In Fig. 18 we show the χ_n^B for $n = 4, 6$ and 8 as functions of the upper limit of the summation k_{max} in Eq. (29). For a very heavy pion mass, there is almost no difference between χ_n^B computed using the Fourier coefficients of the PQM model and those obtained using the CEM scheme. This is due to the rapid decrease of the higher-order coefficients b_k: substantial differences between the CEM and the true Fourier coefficients appear only at large k. Since these are small, they do not contribute significantly to the cumulants, as indicated, e.g., by the rapid convergence of χ_8^B, shown in Fig. 18.

There are, however, large differences between cumulants of the PQM model and those of the CEM scheme for a physical pion mass. This is due to the higher-order

_____

[4]Note that strictly speaking a mean-field calculation does not yield the correct critical behavior, which leads to divergences in χ_6^B and χ_8^B in the chiral limit. However, with a small explicit symmetry breaking term, the mean-field approximation yields baryon number cumulants that are in qualitative agreement with the expected behavior.

[5]We note that for cumulants, where the highest power of k in the corresponding Fourier coefficient, $b_k k^{2n-1}$, is a non-negative integer, the Fourier series diverges due to δ-functions or derivatives thereof at the integration boundaries, $\theta_B = \pm\pi$.

coefficients, which in this case contribute substantially to the χ_n^B. While the CEM cumulants converge rapidly with k, the convergence of the PQM model results is much slower. In the latter, the asymptotic values of χ_6^B and χ_8^B are, at $T = T_{pc}$, reached for $k_{\max} = 10$ and 15, respectively.

The partial sums for the sixth- and eighth-order cumulants shown in Fig. 18 clearly demonstrate that, for a physical m_π, the negative values of these cumulants at $T \simeq T_{pc}$ are by and large due to the large negative values of b_3 and b_4 (see the left panel of Fig. 13). With increasing temperature, the frequency of the oscillation increases, leading to the staggered sign structure and strong cancellations in the sum of Fourier coefficients in Eq. (29). Consequently, at temperatures above T_{pc}, the cumulants χ_6^B and χ_8^B rapidly approach zero, as seen in Fig. 17.

IV. CONCLUDING REMARKS

We have discussed the behavior of the Fourier coefficients of the net baryon density and their relation to the singularities in the complex chemical potential plane.

We found that the presence of singularities is reflected in the asymptotic behavior of the Fourier coefficients. This implies, e.g., that the existence or nonexistence of a phase transition cannot be settled by examining only a few low-order terms in the Fourier series. This was illustrated by considering the cluster expansion model [41]. There, the authors have introduced the phenomenological prescription for computing the higher-order Fourier coefficients b_n of the net baryon density in terms of the first two coefficients, adopted from lattice QCD calculations. Furthermore we have also introduced the model (FRM) for b_n with b_1 and b_2 taken as input parameters from LQCD. In both models, it was demonstrated that knowledge of the first four b_n's is not sufficient to draw any conclusion on criticality. Moreover, considering the analytic structure of CEM we have shown explicitly that the Fourier series of this model can be resummed and expressed by the polylogarithm functions which have well-defined analytic structure. In contrast to the expectation in Ref. [41], this excludes explicitly in CEM any information on the QCD phase transition.

In order to explore the influence of singularities associated with the chiral phase transition on the Fourier coefficients, we employed the PQM model as a low-energy effective approximation to QCD.

We then showed that the large-order behavior of the Fourier coefficients exhibits characteristic oscillations and

exponential damping, due to the imaginary and real parts of the chiral singularity, respectively. Consequently, in the chiral limit, the Fourier coefficients at temperatures $T \leq T_c$ show only an exponential decay, while at $T > T_c$ they exhibit a power-law decay superimposed on oscillations, whose frequency reflects the imaginary baryon chemical potential at the location of the critical point. As the pion mass is increased, the critical behavior is weakened because the singularity is removed from the imaginary axis and thus gains a larger real part, resulting in a stronger damping of the Fourier coefficients. Moreover, we have shown that both the Roberge-Weiss transition and the corresponding end point give rise to characteristic power-law decays of the Fourier coefficients.

Based on the characteristics of the Fourier coefficients, we discussed the implications for the higher-order net baryon number cumulants. We pointed out that the signature of the chiral crossover transition in the net baryon number cumulants [15], the sign change around T_{pc}, is related to the oscillatory behavior of Fourier coefficients induced by the chiral branch-point singularity in the complex chemical potential plane.

Our results indicate that the Fourier coefficients provide valuable information on the QCD phase transitions. Thus, lattice QCD calculations of these coefficients will improve our understanding of the phase structure of QCD. General results on the effect of critical singularities on the Fourier coefficients of the net baryon number are reported in Ref. [36].

[1] X. Luo, Nucl. Phys. **A956**, 75 (2016).

[2] S. Ejiri, F. Karsch, and K. Redlich, Phys. Lett. B **633**, 275 (2006).

[3] F. Karsch, Nucl. Phys. **A967**, 461 (2017).

[4] A. Bazavov *et al.* (HotQCD Collaboration), Phys. Rev. D **96**, 074510 (2017).

[5] F. Karsch, B. J. Schaefer, M. Wagner, and J. Wambach, Phys. Lett. B **698**, 256 (2011).

[6] V. Skokov, B. Friman, and K. Redlich, Phys. Rev. C **83**, 054904 (2011).

[7] M. A. Stephanov, Phys. Rev. Lett. **102**, 032301 (2009).

[8] M. A. Stephanov, Phys. Rev. Lett. **107**, 052301 (2011).

[9] G. A. Almási, B. Friman, and K. Redlich, Phys. Rev. D **96**, 014027 (2017).

[10] A. Bazavov *et al.* (HotQCD Collaboration), Phys. Rev. D **86**, 034509 (2012).

[11] S. Borsanyi, Z. Fodor, S. D. Katz, S. Krieg, C. Ratti, and K. Szabo (Wuppertal-Budapest Collaboration), J. High Energy Phys. 01 (2012) 138.

[12] T. Ichihara, K. Morita, and A. Ohnishi, Prog. Theor. Exp. Phys. **2015**, 113D01 (2015).

[13] C. Sasaki, B. Friman, and K. Redlich, Phys. Rev. D **75**, 054026 (2007).

[14] V. Skokov, B. Stokic, B. Friman, and K. Redlich, Phys. Rev. C **82**, 015206 (2010).

[15] B. Friman, F. Karsch, K. Redlich, and V. Skokov, Eur. Phys. J. C **71**, 1694 (2011).

[16] G. A. Almási, W. Tarnowski, B. Friman, and K. Redlich, Phys. Rev. D **95**, 014007 (2017).

[17] M. Asakawa and M. Kitazawa, Prog. Part. Nucl. Phys. **90**, 299 (2016).

[18] S. Muroya, A. Nakamura, C. Nonaka, and T. Takaishi, Prog. Theor. Phys. **110**, 615 (2003).

[19] P. de Forcrand, Proc. Sci. LAT2009 (**2009**) 010.

[20] P. de Forcrand and O. Philipsen, Nucl. Phys. **B642**, 290 (2002).

[21] P. de Forcrand and O. Philipsen, Nucl. Phys. **B673**, 170 (2003).

[22] M. D'Elia and M. P. Lombardo, Phys. Rev. D **67**, 014505 (2003).

[23] S. Ejiri, Phys. Rev. D **78**, 074507 (2008).

[24] K. Nagata, K. Kashiwa, A. Nakamura, and S. M. Nishigaki, Phys. Rev. D **91**, 094507 (2015).

[25] D. Boyda, V. G. Bornyakov, V. Goy, A. Molochkov, A. Nakamura, A. Nikolaev, and V. I. Zakharov, arXiv: 1704.03980.

[26] V. G. Bornyakov, D. Boyda, V. Goy, A. Molochkov, A. Nakamura, A. Nikolaev, and V. I. Zakharov, EPJ Web Conf. **175**, 07027 (2018).

[27] P. Braun-Munzinger, B. Friman, F. Karsch, K. Redlich, and V. Skokov, Phys. Rev. C **84**, 064911 (2011).

[28] P. Braun-Munzinger, B. Friman, F. Karsch, K. Redlich, and V. Skokov, Nucl. Phys. **A880**, 48 (2012).

[29] K. Morita, V. Skokov, B. Friman, and K. Redlich, Eur. Phys. J. C **74**, 2706 (2014).

[30] K. Morita, B. Friman, K. Redlich, and V. Skokov, Phys. Rev. C **88**, 034903 (2013).

[31] K. Morita, B. Friman, and K. Redlich, Phys. Lett. B **741**, 178 (2015).

[32] A. Nakamura and K. Nagata, Prog. Theor. Exp. Phys. **2016**, 033D01 (2016).

[33] K. Morita and A. Nakamura, Phys. Rev. D **92**, 114507 (2015).

[34] K. Kashiwa and A. Ohnishi, Phys. Rev. D **93**, 116002 (2016).

[35] K. Kashiwa and A. Ohnishi, arXiv:1712.06220.

[36] G. Almási, B. Friman, K. Morita, P. M. Lo, and K. Redlich, Phys. Lett. B **793**, 19 (2019).

[37] B. J. Schaefer, J. M. Pawlowski, and J. Wambach, Phys. Rev. D **76**, 074023 (2007).

[38] K. Morita, V. Skokov, B. Friman, and K. Redlich, Phys. Rev. D **84**, 074020 (2011).

[39] A. Roberge and N. Weiss, Nucl. Phys. **B275**, 734 (1986).

[40] V. Vovchenko, A. Pasztor, Z. Fodor, S. D. Katz, and H. Stoecker, Phys. Lett. B **775**, 71 (2017).

[41] V. Vovchenko, J. Steinheimer, O. Philipsen, and H. Stoecker, Phys. Rev. D **97**, 114030 (2018).

[42] G. N. Mercer and A. J. Roberts, SIAM J. Appl. Math. **50**, 1547 (1990).

[43] K. Fukushima, Phys. Lett. B **591**, 277 (2004).

[44] C. Ratti, M. A. Thaler, and W. Weise, Phys. Rev. D **73**, 014019 (2006).

[45] Y. Sakai, K. Kashiwa, H. Kouno, and M. Yahiro, Phys. Rev. D **77**, 051901(R) (2008).

[46] K. Morita, V. Skokov, B. Friman, and K. Redlich, Phys. Rev. D **84**, 076009 (2011).

[47] V. Skokov, B. Friman, E. Nakano, K. Redlich, and B. J. Schäfer, Phys. Rev. D **82**, 034029 (2010).

[48] Y. Sakai, K. Kashiwa, H. Kouno, M. Matsuzaki, and M. Yahiro, Phys. Rev. D **79**, 096001 (2009).

[49] P. de Forcrand and O. Philipsen, Phys. Rev. Lett. **105**, 152001 (2010).

[50] C. Bonati, M. D'Elia, M. Mariti, M. Mesiti, F. Negro, and F. Sanfilippo, Phys. Rev. D **93**, 074504 (2016).

[51] V. Skokov, K. Morita, and B. Friman, Phys. Rev. D **83**, 071502(R) (2011).

[52] B. Friman, Acta Phys. Pol. B **5**, 707 (2012).

[53] M. Stephanov, Phys. Rev. D **73**, 094508 (2006).

[54] S. Borsányi, Z. Fodor, C. Hoelbling, S. D. Katz, S. Krieg, C. Ratti, and K. K. Szabó, J. High Energy Phys. 09 (2010) 073.

[55] A. Bazavov, T. Bhattacharya, M. Cheng, C. DeTar, H. T. Ding, S. Gottlieb, R. Gupta, P. Hedge, U. M. Heller, F. Karsch *et al.*, Phys. Rev. D **85**, 054503 (2012).